

A Spatial-channel-temporal-fused Attention for Spiking Neural Networks

Wuque Cai, Hongze Sun, Rui Liu, Yan Cui, Jun Wang, Yang Xia, Dezhong Yao, *Senior Member, IEEE*, and Daqing Guo

Abstract—Spiking neural networks (SNNs) mimic brain computational strategies, and exhibit substantial capabilities in spatiotemporal information processing. As an essential factor for human perception, visual attention refers to the dynamic selection process of salient regions in biological vision systems. Although mechanisms of visual attention have achieved great success in computer vision, they are rarely introduced into SNNs. Inspired by experimental observations on predictive attentional remapping, we here propose a new spatial-channel-temporal-fused attention (SCTFA) module that can guide SNNs to efficiently capture underlying target regions by utilizing historically accumulated spatial-channel information. Through a systematic evaluation on three event stream datasets (DVS Gesture, SL-Animals-DVS and MNIST-DVS), we demonstrate that the SNN with the SCTFA module (SCTFA-SNN) not only significantly outperforms the baseline SNN (BL-SNN) and other two SNN models with degenerated attention modules, but also achieves competitive accuracy with existing state-of-the-art methods. Additionally, our detailed analysis shows that the proposed SCTFA-SNN model has strong robustness to noise and outstanding stability to incomplete data, while maintaining acceptable complexity and efficiency. Overall, these findings indicate that appropriately incorporating cognitive mechanisms of the brain may provide a promising approach to elevate the capability of SNNs.

Index Terms—Spiking neural networks, Visual attention, Predictive attentional remapping, Spatial-channel-temporal-fused attention, Event streams.

I. INTRODUCTION

OVER the past decade, spiking neural networks (SNNs) have received unprecedented attention and have exhibited powerful capabilities in various intelligent scenarios [1]–[3], such as pattern recognition [4], object tracking [5]–[7] and robot navigation [8]–[11]. In SNNs, neural information is represented and transmitted in the form of discrete spike events, and such non-differentiable feature of spikes makes the learning in SNNs to be more difficult than that of conventional

artificial neural networks (ANNs). To overcome this challenge, several training approaches, such as gradient-based optimization [12], [13] and ANN-to-SNN conversion [14], [15], have been developed to endow SNNs with competitive performance. A deep understanding of the computational principles of realistic brain can inspire us to design more efficient SNN models.

Visual attention is a critical cognitive process that enables humans to selectively allocate limited attention resources to underlying targets [16], [17]. Remarkably, recent years have witnessed a great development of visual attention in computer vision, and various types of attention modules in channel [18], [19], spatial [20]–[22], temporal [23], [24] and their combination dimensions [25]–[28] have been designed for different neural network models. Although visual attention has achieved great success in traditional ANN models, these attention-related mechanisms are seldom considered to be introduced into SNNs. Despite this fact, we noticed that a few recent studies showed great potential of visual attention in performance improvement of SNNs [29]–[32]. To the best of our knowledge, however, most of these studies concentrated on attention mechanisms in one or two dimensions, and none of them attempted to combine spatial, channel and temporal information altogether.

There are increasing experimental studies that have revealed a predictive attentional remapping mechanism in the mammalian brain [33]–[38]. By measuring the spatiotemporal change of attention when saccades occur, it has been widely observed that attention can be shifted to the underlying target area before the eyes move toward it [33]–[35], [38]. Further experiments on attention remapping have demonstrated that an accurate predictive remapping highly relies on the spatial and temporal dynamics of attention and requires a sufficient accumulation of spatiotemporal information [36], [37]. Theoretically, these findings provide an efficient approach for predictively shifting attention to areas where the target is possible to arrive based on historical information. Inspired by these experimental findings, we have an intuitive idea that incorporating the concept of predictive attentional remapping into existing attention modules may be helpful for locating underlying target regions.

Accordingly, in this study, we propose a novel spatial-channel-temporal-fused attention (SCTFA) module for SNNs. For this purpose, we employ a three-dimensional (3-D) spatial-channel attention block to capture discriminative spatial-channel information of underlying targets. Then, we introduce the feedback of attention into the temporal evolution of the

This work was supported in part by the MOST 2030 Brain Project under Grant 2022ZD0208500 and in part by the National Natural Science Foundation of China under Grant 61933003, Grant 82072011, and Grant 31771149. (Corresponding authors: Dezhong Yao; Daqing Guo).

Wuque Cai, Hongze Sun, Rui Liu, Yan Cui, Jun Wang, Yang Xia, Daqing Guo are with the Clinical Hospital of Chengdu Brain Science Institute, MOE Key Lab for NeuroInformation, School of Life Science and Technology, University of Electronic Science and Technology of China, Chengdu 611731, China (e-mail: dqguo@uestc.edu.cn).

Dezhong Yao is with the Clinical Hospital of Chengdu Brain Science Institute, MOE Key Lab for NeuroInformation, School of Life Science and Technology, University of Electronic Science and Technology of China, Chengdu 611731, China, also with the Research Unit of NeuroInformation (2019RU035), Chinese Academy of Medical Sciences, Chengdu 611731, China, and also with the School of Electrical Engineering, Zhengzhou University, Zhengzhou 450001, China (e-mail: dyao@uestc.edu.cn).

membrane potentials of neurons (see Methods for details). With this method, the attention tensor has a long-term effect on neuronal membrane potentials, and its historical spatial-channel information is regulated by the decay factor of membrane potentials. For the sake of simplicity, we name the SNN with the SCTFA module as SCTFA-SNN. From the functional perspective, the major novelty of our SCTFA-SNN model is that it can make full use of the accumulated spatial-channel information to determine underlying target regions. To examine the performance of the SCTFA-SNN model, we evaluated and compared it with other SNN models on three benchmark event-stream datasets. Our detailed experiments and analysis clearly demonstrate the superiority of the proposed SCTFA-SNN model on event stream classifications, which can achieve competitive accuracy with existing state-of-the-art (SOTA) methods.

The main contributions of our work are summarized as follows:

- We design an SCTFA module to extract and accumulate spatial-channel information in the temporal (historical) domain. Accordingly, the proposed SCTFA module can make full use of spatial, channel and temporal information for locating targets.
- We introduce a long-term effect of attention tensor on neuronal membrane potentials. In this way, we can realize the concept of predictive remapping of attention with the help of historical spatial and channel information.
- Ablation study shows that the SCTFA-SNN outperforms the baseline SNN (BL-SNN) and other two SNN models with the degenerated spatial-temporal-fused and channel-temporal-fused attention modules.
- The SCTFA-SNN model achieves better or comparable accuracy with other SOTA results on three benchmark even stream datasets, and meanwhile exhibits substantial superiority in robustness and stability to noisy and incomplete data.

The rest of this paper is structured as follows. In the next section, we review the recent development of the training methods and attention mechanisms for SNNs, and introduce the typical strategies for improving the representation of event streams. Then, we describe the neuron model, the structure of the SCTFA module and the learning method for training the SCTFA-SNN models step by step in Section III. Section IV provides the detailed experimental results and analysis of the SCTFA-SNNs on different datasets. Finally, we give a brief conclusion in Section V.

II. RELATED WORK

A. Training methods for SNNs

There are various strategies for SNN training, and the ANN-to-SNN conversion and gradient-based optimization are two fundamental approaches [12]–[15]. As an indirect supervised learning approach, ANN-to-SNN conversion first trains an ANN and then maps parameters to an SNN with an equivalent architecture [14], [15]. For a sufficient inference time, the performance of converted SNNs can achieve near-lossless accuracy. On the other hand, the gradient-based optimization

is a promising supervised learning approach that directly trains SNNs by calculating the gradient through backpropagation (BP). However, because the spike activity is non-differentiable, the true gradient cannot be accurately computed and, therefore, surrogate and approximate gradients are commonly introduced to solve this dilemma [12], [13]. To date, several spike-based BP methods have been derived. Typical methods include, but are not limited to, the spike layer error reassignment in time (SLAYER) [39], the spatiotemporal BP (STBP) [12], and BP through time (BPTT) [40]. Among them, the STBP is believed to be a powerful learning method for highly efficient SNN models, which is also employed in our study to train different SNN models.

B. Attention Mechanisms in SNNs

In computer vision, many types of attention models and modules have been developed to capture underlying regions of interest while neglecting other useless information [18]–[28]. However, compared with ANNs, there are only a few studies that try to involve attention mechanisms in SNN models [29]–[32]. For example, Yao et al. designed a temporal-wise attention module for input frames to obtain their statistical characteristics at different times [29]. With this method, the importance of different frames can be judged during training and the irrelevant frames can be discarded at the inference stage, thus resulting in a substantial performance increase. Recently, several studies further demonstrated the effectiveness of visual attention by introducing spatial-wise, channel-wise and temporal-wise attentions into SNN models [30]–[32]. Inspired by predictive remapping of attention [34]–[38], we attempt to construct a spatial-channel-temporal-fused attention module for SNNs, which allows us to effectively locate underlying target regions by using historically accumulated spatial-channel information. To the best of our knowledge, our proposed SCTFA attention mechanism is the first one that combines the spatial, channel, and temporal information altogether for SNNs.

C. Representation of event streams

We use several event stream datasets recorded by event cameras to assess our models [41]–[43]. As a biological-inspired sensor, an event camera responds to light intensity changes at each pixel of the sensor with high temporal resolution, low energy computation and high dynamic range [44], [45]. For event streams, information is encoded with sparsely asynchronous spatiotemporal events. To improve the information representation of event streams, one mainstream approach is to split event-based data into different slices and convert them into frame-based data. Despite such a frame-based representation discarding sparsity of asynchronous events, it considerably reduces the difficulty of the learning process. Due to relatively high signal-to-noise ratio, the frame-based representation has been widely used for the processing of event streams [29], [46]–[52]. Furthermore, several data augmentation strategies have been recently proposed as a new approach to enhance the representation ability of sparse events. Typical examples are EventMix [53] and EventDrop [54]. However, for a fair

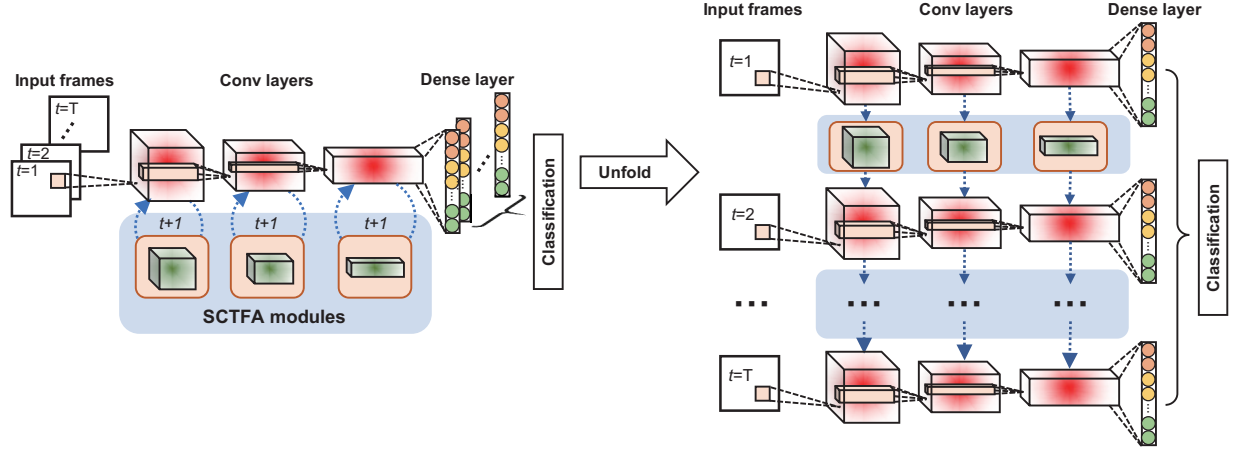


Fig. 1. The architecture and unfolding form of the proposed SCTFA-SNN. The SCTFA module is inserted into each convolutional (Conv) layer and converts the spiking feature maps (SFM) into an attention tensor (blue). SFMs extracted by the last convolutional layer are put into a dense layer for classification.

comparison with other SOTA results on SNN models, we employ the frame-based representation for event streams and do not consider any data augmentation strategy in this work.

III. METHODS

In this section, we first describe the leaky-integrate-and-fire (LIF) neuron model used in this study, then introduce the structure of the SCTFA module and the learning method of SCTFA-SNN models in detail.

A. LIF Neuron Model

A large variety of models have been developed to resemble the spiking dynamics of biological neurons. The LIF neuron model is one of the most commonly used models, which allows us to simulate the dynamics of SNNs in an efficient way [55]. The differential equation of a single LIF model can be described as follows:

$$\tau \frac{dv_i}{dt} = -(v_i - v_{\text{rest}}) + I_i, \quad (1)$$

where v_i is the membrane potential of the i -th neuron, τ is the membrane time constant, v_{rest} is the resting potential, and I_i is the input current from its presynaptic neurons. Whenever the membrane potential of a neuron reaches a threshold at v_{th} , a spike is generated and after that its membrane potential is reset to the resting potential v_{rest} . Mathematically, this process produces a binary spike train $s_i = (s_i^1, \dots, s_i^t, \dots, s_i^T)$ for the i -th neuron, with:

$$s_i^t = g(v_i) = \begin{cases} 1 & \text{if } v_i \geq v_{\text{th}}, \\ 0 & \text{otherwise.} \end{cases} \quad (2)$$

Without loss of generality, we set $v_{\text{rest}} = 0$ mV and derive a simple iterative form of the LIF neuron model as follows:

$$v_i^{t+1} = \kappa_\tau v_i^t (1 - s_i^t) + \frac{dt}{\tau} I_i(t), \quad (3)$$

where v_i^t and $I_i(t)$ are the membrane potential and synaptic input of the i -th neuron at time t , dt represents the integration time step, and $\kappa_\tau = 1 - \frac{dt}{\tau}$ is a decay factor. By eliminating

the scaling effect $\frac{dt}{\tau}$ into the synaptic weights, we obtain the final iterative formula of the LIF neuron model as follows:

$$v_i^{t+1} = \kappa_\tau v_i^t (1 - s_i^t) + \sum_j w_{ij} s_j^{t+1}, \quad (4)$$

where the outer sum runs over all synapses onto the i -th neuron, and w_{ij} is the scaled synaptic weight from the j -th neuron to the i -th neuron.

B. Structure of the SCTFA Module

We employ SNNs with convolutional structures and frame-based representation for event stream processing. As the network architecture shown in Fig. 1 (left), we insert an SCTFA module into each convolutional layer to convert the spiking feature maps (SFMs). For each convolutional layer, the SFMs at time t are converted into an attention tensor that affects the same layer at time $t + 1$. This attention module transfers spatial-channel information through time that constitutes the basic structure of the SCTFA module. The SFMs extracted by the last convolutional layer are put into a dense layer for voting with a rate-based decoding strategy. For a more clear understanding, the unfolding structure of the SCTFA-SNN is also schematically depicted in Fig. 1 (right).

In the SCTFA module, the SFMs are transferred by an attention block to generate an attention tensor with the same size [Fig. 2]. To do this, a spatial-channel attention block (3-D), consisting of a spatial attention block (2-D) and a channel attention block (1-D), is designed to extract the information of output SFMs [25], [56]. Mathematically, we define the output SFMs of the l -th convolutional layer at time t represented by the binary spiking tensor $\mathbf{S}^{t,l}$ with size of $H \times W \times C$, where C is the number of channels, and H and W are the height and width of the SFMs. In this study, the spatial attention block is generated by channel squeeze spatial excitation through the convolution and nonlinear transformation of SFMs as follows [56]:

$$\mathbf{U}_{\text{sSE}}^{t,l} = \sigma(\mathbf{W}_s^l * \mathbf{S}^{t,l} + b^l), \quad (5)$$

where $\sigma(\cdot)$ is the sigmoid function, $\mathbf{W}_s^l \in \mathbb{R}^{1 \times 1 \times C \times 1}$ and $b^l \in \mathbb{R}$ are the weight matrix of the kernel and the bias vector

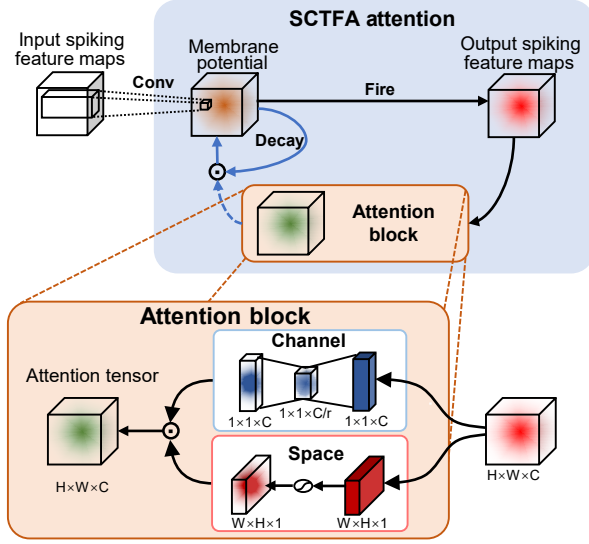


Fig. 2. Diagram of the SCTFA module. The attention block of the SCTFA module is composed of both channel and spatial attention blocks. This attention block generates a 3-D attention tensor that excites corresponding neurons at the same layer, with its historical influence adjusted by the decay factor of membrane potentials.

of the convolution, respectively, and $\mathbf{U}_{\text{SE}}^{t,l} \in \mathbb{R}^{1 \times H \times W}$ is the spatial attention tensor representing the relative weight in the spatial direction. On the other hand, the channel attention block is acquired by spatial squeeze channel excitation. For this purpose, we first perform a squeeze operation in the spatial direction:

$$\mathbf{e}^{t,l} = \frac{1}{H \times W} \sum_{i=1}^H \sum_{j=1}^W \mathbf{S}^{t,l}(i, j), \quad (6)$$

where $\mathbf{e}^{t,l} \in \mathbb{R}^{C \times 1 \times 1}$ is the average channel vector in the spatial direction. Then, channel excitation can be achieved by using two fully connected nonlinear transformations as follows [18]:

$$\mathbf{U}_{\text{cSE}}^{t,l} = \sigma(\mathbf{W}_{\text{c2}}^l \cdot \delta(\mathbf{W}_{\text{c1}}^l \mathbf{e}^{t,l})), \quad (7)$$

where $\delta(\cdot)$ is the ReLU function, $\mathbf{W}_{\text{c1}}^l \in \mathbb{R}^{\frac{C}{r} \times C}$ and $\mathbf{W}_{\text{c2}}^l \in \mathbb{R}^{C \times \frac{C}{r}}$ are the weights of the linear function with a reduction ratio of r , and $\mathbf{U}_{\text{cSE}}^{t,l} \in \mathbb{R}^{C \times 1 \times 1}$ is the channel attention tensor denoting the relative weight in the channel direction.

We generate an overall 3-D attention tensor by combining above spatial and channel attention tensors as follows:

$$\mathbf{U}_{\text{SE}}^{t,l} = \mathbf{U}_{\text{sSE}}^{t,l} (\mathbf{S}^{t,l}) \odot \mathbf{U}_{\text{cSE}}^{t,l} (\mathbf{S}^{t,l}), \quad (8)$$

where \odot is the Hadamard product, and $\mathbf{U}_{\text{SE}}^{t,l} \in \mathbb{R}^{C \times H \times W}$ denotes the 3-D attention tensor of SFMs. Each element within this tensor corresponds to a neuron in SFMs, and its value refers to the importance level of the neuron at time t . To achieve a long-term influence process, we integrate the feedback of the 3-D attention tensor into the membrane potentials of neurons and rewrite the iterative formula of the LIF neuron model in the SCTFA-SNN as follows:

$$v_i^{t+1,l} = \kappa_{\tau} v_i^{t,l} u_{\text{SE};i}^{t,l} (1 - s_i^{t,l}) + \sum_j w_{ij}^{l,l-1} s_j^{t+1,l-1}, \quad (9)$$

where $s_i^{t,l}$ and $v_i^{t,l}$ are binary spike and membrane potential of the i -th neuron in the l -th layer at time t , $u_{\text{SE};i}^{t,l} \in \mathbf{U}_{\text{SE}}^{t,l}$ is the corresponding attention value, and $w_{ij}^{l,l-1}$ is synaptic weight from the j -th neuron in the $(l-1)$ -th layer to the i -th neuron in the l -th layer. Theoretically, the decay factor of neuronal membrane determines the impact of historical information on the current influence. From the functional perspective, the SCTFA-SNN uses historically accumulated spatial-channel information to capture the underlying targets.

C. Learning Method

In this study, we use a rate-based decoding strategy for event stream classification. To this end, we consider the last layer in SNN as the voting layer that is composed of M classes with each class represented by P neurons. For a given input with the m -th class, we encourage neurons representing this class to have the highest spiking activity. Thus, the output vector $\mathbf{o}^t = \{o_1^t, o_2^t, \dots, o_m^t, \dots, o_M^t\}$ at time t can be calculated as follows:

$$o_m^t = \frac{1}{P} \sum_{i=(m-1)P}^{mP} s_i^{t,L}, \quad (10)$$

where o_m^t is the average spiking events of neurons in the m -th class at time t . Then, the loss function is described by the mean squared error:

$$\text{Loss} = \frac{1}{2N} \sum_{n=1}^N \left\| \mathbf{Y}_n - \frac{1}{T} \sum_{t=1}^T \mathbf{o}_n^t \right\|_2^2. \quad (11)$$

Here \mathbf{o}_n^t represents the average voting vector at timestep t , \mathbf{Y}_n denotes the label vector of input data, N is the number of training samples, and T is the total timestep of simulations.

We use the STBP method to train the SNN models [12], [13]. In the STBP method, the gradient of the loss function L with respect to $s_i^{t,l}$ and $v_i^{t,l}$ can be calculated as follows:

$$\frac{\partial \text{Loss}}{\partial s_i^{t,l}} = \sum_{j=1}^{n^{l+1}} \frac{\partial \text{Loss}}{\partial s_j^{t,l+1}} \frac{\partial s_j^{t,l+1}}{\partial s_i^{t,l}} + \frac{\partial \text{Loss}}{\partial s_i^{t+1,l}} \frac{\partial s_i^{t+1,l}}{\partial s_i^{t,l}}, \quad (12)$$

$$\frac{\partial \text{Loss}}{\partial v_i^{t,l}} = \frac{\partial \text{Loss}}{\partial s_i^{t,l}} \frac{\partial s_i^{t,l}}{\partial v_i^{t,l}} + \frac{\partial \text{Loss}}{\partial s_i^{t+1,l}} \frac{\partial s_i^{t+1,l}}{\partial v_i^{t,l}}. \quad (13)$$

In this study, a surrogate function is utilized to approximate the activation of discrete spikes [12], [13]:

$$g(v_i^{t,l}) = \frac{1}{\pi} \arctan \left[\frac{\pi}{2} \alpha (v_i^{t,l} - v_{\text{th}}) \right] + \frac{1}{2}, \quad (14)$$

where a factor of $\alpha = 2$ is used to adjust the slope of the surrogate function near zero.

However, learning in the SCTFA module cannot be directly accomplished with the standard STBP method [12], [13]. When inputting the SFMs of the l -th layer at time t into the SCTFA module, an attention tensor is introduced to adjust the membrane potentials of neurons in the l -th layer at time $t+1$. In this case, the gradient in the SCTFA module with respect to $u_{\text{SE};i}^{t,l}$ and $s_i^{t,l}$ can be written as follows:

$$\frac{\partial s_i^{t+1,l}}{\partial u_{\text{SE};i}^{t,l}} = \frac{\partial s_i^{t+1,l}}{\partial v_i^{t+1,l}} \kappa_{\tau} v_i^{t,l} (1 - s_i^{t,l}), \quad (15)$$

Algorithm 1 Training of the SCTFA-SNN model.

Require: Input sample $\{\mathbf{S}^{t,0}\}_{t=1}^T$, target label Y , parameters of synaptic weights and SCTFA modules of each layer ($\mathbf{W}^l, \mathbf{W}_{c1}^l, \mathbf{W}_{c2}^l, \mathbf{W}_s^l, \mathbf{b}^l$) $_{l=1}^L$, states of membrane potential and spike train of each layer ($\mathbf{V}^{t,l}, \mathbf{S}^{t,l}$), spike counter of SNN \mathbf{o}^L , and 1-D average pooling (AP) // Calculating network output from voting layer.

Ensure: Updated parameter $\mathbf{W}^l, \mathbf{W}_{c1}^l, \mathbf{W}_{c2}^l, \mathbf{W}_s^l$ and \mathbf{b}^l

for $l = 1$ to $L + 1$ **do**

$\mathbf{V}^{1,l}, \mathbf{S}^{1,l} \leftarrow \text{StateUpate}(\mathbf{V}^{1,l}, \mathbf{S}^{1,l-1}, \mathbf{W}^l)$ // Eqs. (2)-(4)

end for

for $t = 2$ to T **do**

for $l = 1$ to $L + 1$ **do**

if ConvLayer **then**

$\mathbf{U}_{SE}^{t,l} \leftarrow \text{FusedAttention}(\mathbf{U}_{sSE}^{t,l}, \mathbf{U}_{cSE}^{t,l})$ // Eqs. (5)-(8)

$(\mathbf{V}^{t,l}, \mathbf{S}^{t,l}) \leftarrow \text{StateUpate}(\mathbf{S}^{t,l-1}, \mathbf{V}^{t,l}, \mathbf{S}^{t-1,l}, \mathbf{U}_{SE}^{t,l}, \mathbf{W}^l)$ // Eq. (9)

else

$(\mathbf{V}^{t,l}, \mathbf{S}^{t,l}) \leftarrow \text{StateUpate}(\mathbf{V}^{t,l}, \mathbf{S}^{t-1,l}, \mathbf{W}^l)$

end if

end for

$\mathbf{o}^L \leftarrow \mathbf{o}^L + \mathbf{S}^{t,L}$ // Calculating the number of voting spikes.

end for

$\mathbf{p} \leftarrow \text{AP}(T, \mathbf{o}^L)$ // Eq. (10)

$\text{Loss} \leftarrow \text{MSE}(\mathbf{Y}, \mathbf{p})$ // Eq. (11)

Update $\{\mathbf{W}^l, \mathbf{W}_{c1}^l, \mathbf{W}_{c2}^l, \mathbf{W}_s^l, \mathbf{b}^l\}_{l=1}^L$ // Eqs. (11)-(16)

$$\frac{\partial u_{SE,i}^{t,l}}{\partial s_i^{t,l}} = u_{sSE,i}^{t,l} \frac{\partial u_{cSE,i}^{t,l}}{\partial s_i^{t,l}} + u_{cSE,i}^{t,l} \frac{\partial u_{sSE,i}^{t,l}}{\partial s_i^{t,l}}. \quad (16)$$

With Eqs.(11)-(16), we can efficiently train the proposed SCTFA-SNN model [see Algorithm 1]. By removing the channel or spatial block from the SCTFA module, our model is degenerated into an SNN with the spatial-temporal-fused attention (STFA-SNN) or the channel-temporal-fused attention (CTFA-SNN).

IV. EXPERIMENTS

A. Datasets and Implementations

In this study, we test our models on three benchmark event stream datasets, including two gesture recognition datasets (DVS Gesture [41] and SL-Animals-DVS [42]) and one converted DVS dataset (MNIST-DVS [43]). All these datasets are recorded by event cameras, and have a spatial resolution of 128×128 pixels, with two channels representing positive and negative changes in scene illumination. For each event stream data, we split it into different slices with a fixed length of Δt , and chose the first T slices as training and test data. Then, we accumulate spike trains for each slice and feed them into the SNNs. The detailed descriptions of these event stream datasets are given as follows.

DVS Gesture: The DVS Gesture contains 11 different gestures recorded from 29 different individuals. These data are captured by an Inilabs DVS camera under three different lighting conditions. In the DVS gesture dataset, the default numbers of training and test samples are 1176 and 288, respectively.

SL-Animals-DVS: The SL-Animals-DVS is a more challenging dataset for gesture recognition. Briefly, this dataset

TABLE I
DEFAULT VALUES OF HYPERPARAMETERS FOR DIFFERENT DATASETS.

Dataset	DVS Gesture	SL-Animals-DVS	MNIST-DVS
Epoch	200	200	100
Batch Size	16	25	100
η	0.002	0.0002	0.001
γ	0.98	0.97	0.95
v_{th} (mV)	1.15	1.5	0.8
κ_τ	0.7	0.4	0.5
r	4	4	4
T	10	30	20
Δt (ms)	125	50	25
L (ms)	1250	1500	500

TABLE II
ARCHITECTURES OF SNN MODELS FOR DIFFERENT DATASETS.

Dataset	Network Architecture
DVS Gesture	Input-128C5S2-BN-AP2-128C3-BN-AP2-128C3-BN-AP2-128C3-BN-AP2-512FC-VotingC11P5-AP
SL-Animals-DVS	Input-128C5S2-BN-AP2-128C3-BN-AP2-128C3-BN-AP2-DP-512FC-DP-VotingC19P5-AP
MNIST-DVS	Input-32C7S2-BN-AP2-64C3-BN-AP2-128C3-BN-AP2-512FC-VotingC10P5-AP

is a collection of 1121 samples captured by 58 different subjects performing 19 types of sign language gestures under four collection environments (4 sets). In our experiments, we randomly choose 840 and 281 event streams as training and test samples.

MNIST-DVS: The MNIST-DVS is composed of 30000 DVS handwritten digital data recorded from the MNIST. There are three recording scales (4, 8 and 16) in the MNIST-DVS, and the total number of data sets for each scale is 10000. We choose the scale of 4 and set the ratio of the training and test sets as 9:1 in experiments.

All experiments are conducted on a workstation equipped with NVIDIA V100 GPUs. The computer codes of our SNN models are implemented by using the PyTorch framework. During the training phase, we combine the Adam optimizer with an exponential decay strategy (initial learning rate η and decay factor γ). Unless otherwise stated, we use the default hyperparameters listed in Tab. I in our experiments. Note that, however, there are a few event streams with their actual lengths less than the required total length ($L = \Delta t \cdot T$). For these event streams, we use the zero-padding method at the end of frame-based inputs to maintain the number of slices as T . On different datasets, we construct SNNs with their detailed network architectures given in Tab. II. For example, we train a 7-layer spiking CNN for the SL-Animals-DVS, with its architecture: [Input-128C5S2-BN-AP2-128C3-BN-AP2-128C3-BN-AP2-128C3-BN-AP2-128C3-BN-AP2-DP-512FC-DP-VotingC19P5-AP]. Here, 128C5S2 refers to the convolutional layer with (channel, kernel size, stride) = (128, 5, 2), BN represents the batch normalization, and AP2 means a 2×2 average pool. DP means dropout with a rate of 0.5. 512FC denotes a fully connected layer with 512

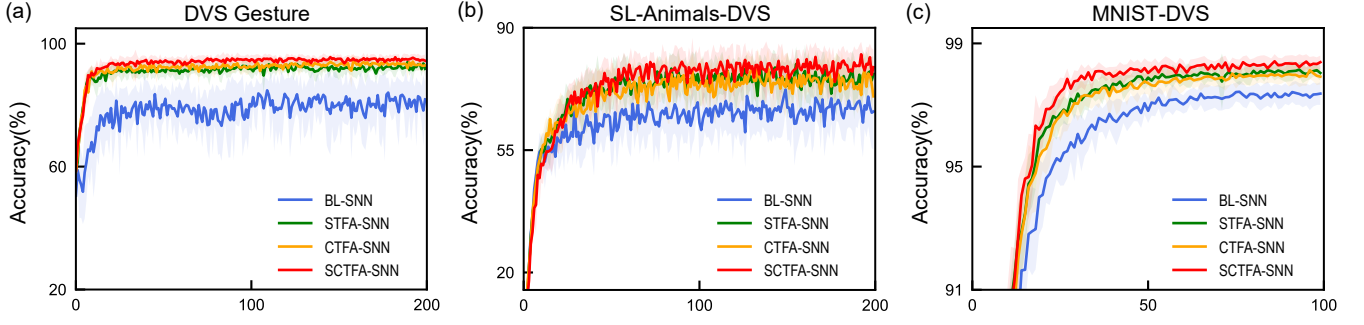


Fig. 3. Average training curves of different SNN models on three datasets. (a) DVS Gesture, (b) SL-Animals-DVS and (c) MNIST-DVS. Different colors represent different SNN models: BL-SNN (blue), STFA-SNN (green), CTFA-SNN (orange) and SCTFA-SNN (red).

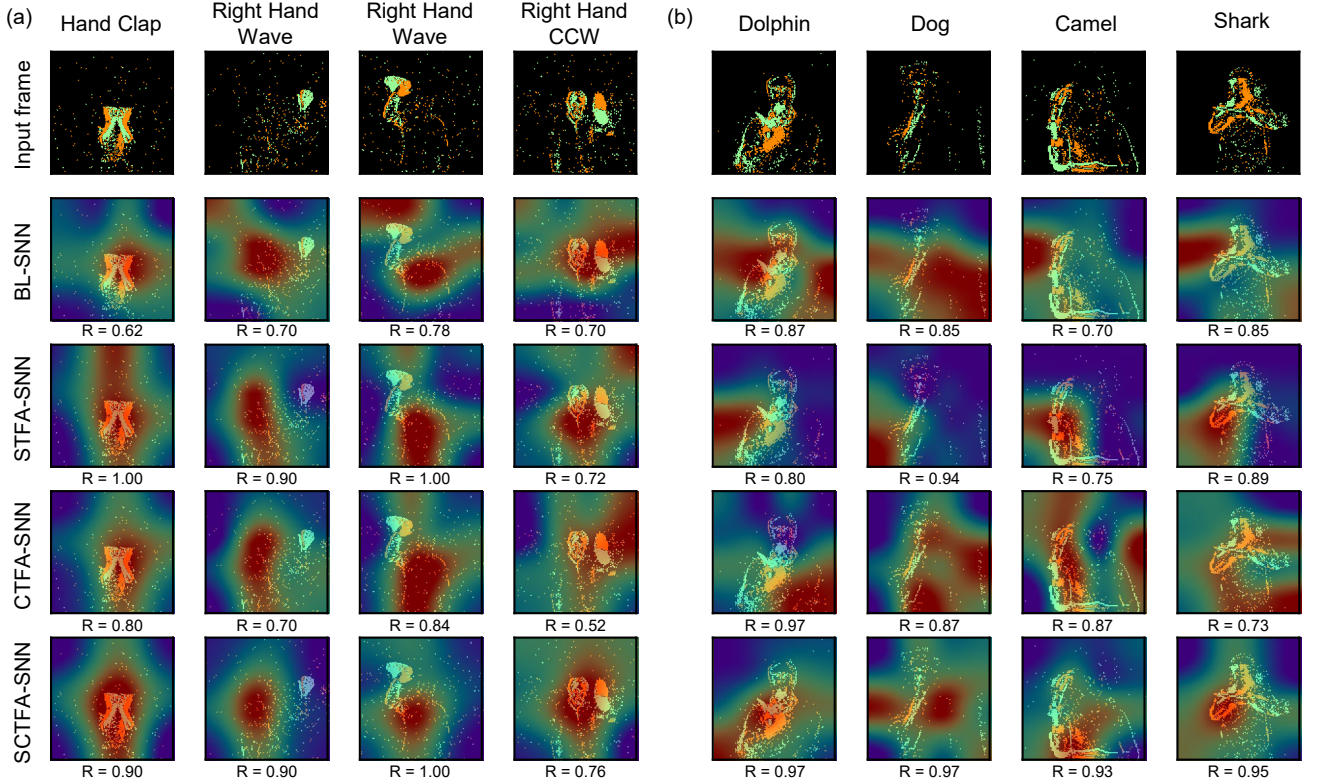


Fig. 4. Visualization of input frames of typical samples and their corresponding attentional heatmaps captured by the BL-SNN, STFA-SNN, CTFA-SNN and SCTFA-SNN models. (a) DVS Gesture and (b) SL-Animals-DVS. R indicates the average firing ratio in the target class at the voting layer during the inference phase.

output features. VotingC19P5 indicates 19 output classes in the voting layer with 5 neurons for each class. For each experimental setting, we repeat 10 independent trials, and report the average (mean \pm standard deviation) and the best top-1 accuracy as final results.

B. Ablation Study

We conduct ablation experiments to verify the effectiveness of the proposed method. For a fair evaluation, we train SNNs with different types of attention modules (STFA-SNN, CTFA-SNN, and SCTFA-SNN) and the baseline SNN (BL-SNN) without any attention module on each dataset. In Fig. 3, we plot the average training curves of different SNN models. On all datasets, the SCTFA-SNN model has relatively fast

convergence speed and displays the best average performance. To further compare the accuracy of different SNN models in detail, we summarize the average and best top-1 accuracy over 10 trials in Tab. III. As we see, introducing the historically accumulated channel and spatial information can both improve the baseline performance. However, the STFA-SNN model exhibits slighter higher accuracy than the CTFA-SNN model on two gesture datasets acquired in natural scenes, whereas both of them can achieve the similar performance on the MNIST-DVS. Further comparison reveals that the SCTFA-SNN model significantly outperforms these two degenerated SNN models across all datasets. Theoretically, this is because the SCTFA-SNN model can make full use of the spatial-channel information accumulated in the temporal domain.

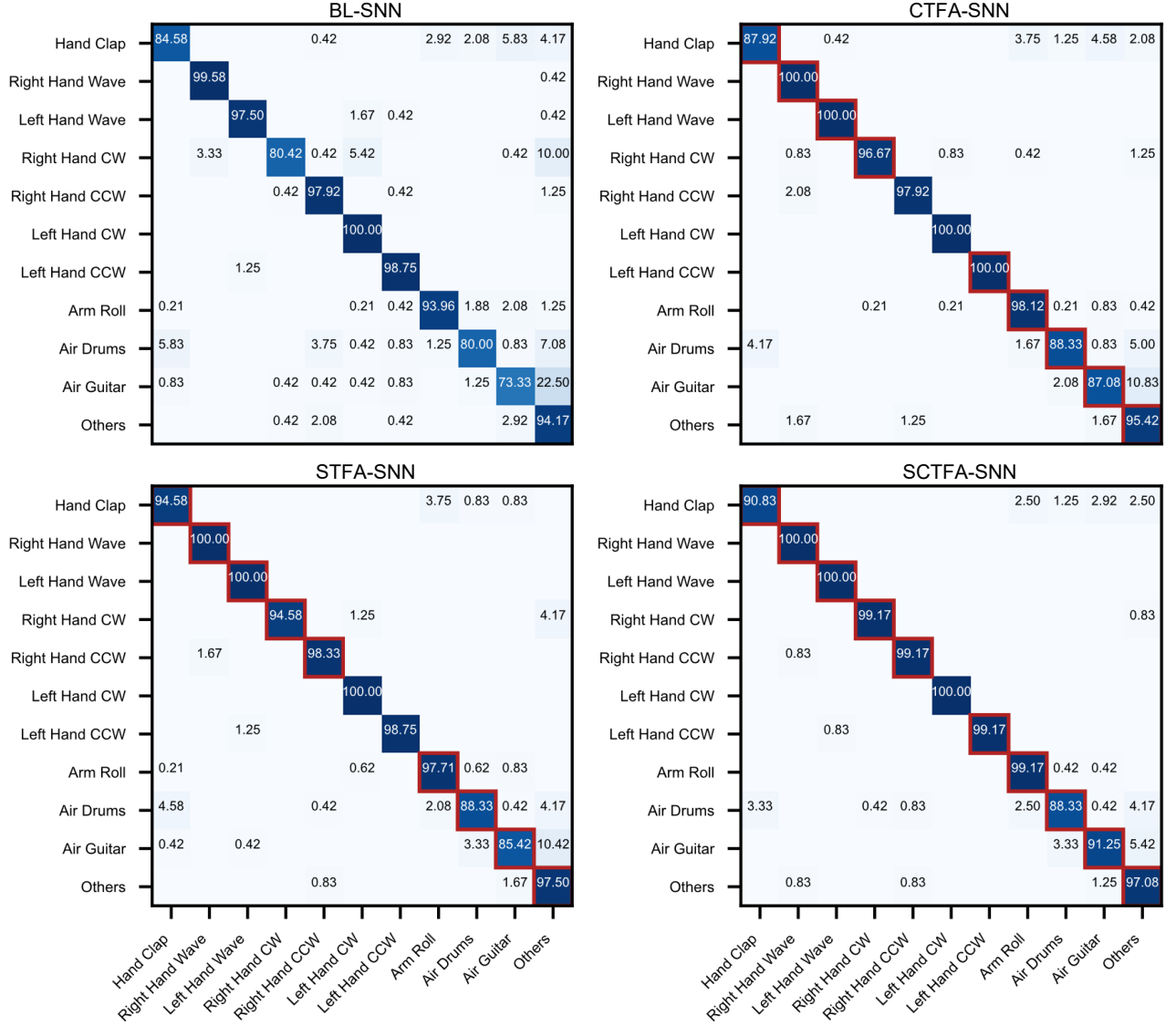


Fig. 5. Average confusion matrices of different SNN models on the DVS Gesture. CW: Clockwise; CCW: Counter Clockwise. The data presented in the confusion matrices are percentages (%). Compared with the BL-SNN model, red boxes on primary diagonal of the confusion matrices denote that the recognition rates of corresponding gestures are increased.

In particular, we find that the superiority of the SCTFA-SNN is noticeable for tasks with complicated spatio-temporal features. In comparison with the BL-SNN model, the average and best top-1 accuracies of the SCTFA-SNN model are improved 6.46% and 4.86% on the DVS Gesture, and 5.09% and 4.63% on the challenging SL-Animals-DVS [Tab. III]. For the simplest MNIST-DVS, we only observe 1.00% and 0.70% improvement in the average and best top-1 accuracies [Tab. III], respectively.

To qualitatively analyze the role of the SCTFA module, we apply Gradient-weighted Class Activation Mapping++ (Grad-CAM++) [57] to identify the attentional locations for different SNN models. Briefly, Grad-CAM++ is an advanced visualization method that uses weighted combination of positive gradients to compute the importance of the spatial locations in convolutional layers [57]. Figure 4 shows attentional visualization results of typical samples in the DVS Gesture and SL-Animals-

DVS. The red color in the generated heatmap denotes valuable regions captured by the Grad-CAM++ method. Compared with the BL-SNN model, it is obvious that the attention regions of SNNs with different types of attention modules are much more focused on the human body. By further computing the average firing ratio R for neurons in the target class at the voting layer, we confirm that the SCTFA-SNN model exhibits considerably larger R values than both the STFA-SNN and CTFA-SNN models, thus indicating its stronger capability in locating targets [Fig. 4].

For a more insightful analysis, we calculate the average confusion matrices of different SNN models on the DVS Gesture. The corresponding results are illustrated in Fig. 5. Compared with the BL-SNN model, we find that the accuracies of nine gestures are improved for both the STFA-SNN and CTFA-SNN models. As expected, the SCTFA-SNN model exhibits much higher recognition rates for almost all

TABLE III
AVERAGE TOP-1 ACCURACY (UPPER) AND BEST TOP-1 ACCURACY (BOTTOM) OF BL-SNN, STFA-SNN, CTFA-SNN AND SCTFA-SNN MODELS ON DIFFERENT DATASETS.

Model	DVS Gesture	SL-Animals-DVS	MNIST-DVS
BL-SNN	90.87 \pm 1.41% 93.06%	81.46 \pm 2.59% 85.41%	97.72 \pm 0.25% 98.20%
STFA-SNN	96.04 \pm 1.28% 97.57%	85.44 \pm 1.95% 88.97%	98.30 \pm 0.26% 98.90%
CTFA-SNN	96.01 \pm 0.64% 97.22%	84.56 \pm 1.74% 87.90%	98.40 \pm 0.22% 98.70%
SCTFA-SNN	97.33 \pm 0.58% 97.92%	86.55 \pm 1.64% 90.04%	98.72 \pm 0.14% 98.90%

classes (ten gestures) in comparison with the BL-SNN, and keeps the 100% classification accuracy as that of other SNN models for the “Left Hand CW” [Fig. 5]. Indeed, the SCTFA-SNN model can achieve and maintain the best performance on eight gestures among all SNN models, thus leading to a more significant improvement in the performance on the DVS Gesture. Note that, in additional experiments, we also observe the similar results on both the SL-Animals-DVS and MNIST-DVS datasets (data not shown).

Overall, these findings indicate that the SCTFA module can help SNNs to exploit information in appropriate attention regions, thus equipping them with competitive performance for event stream classifications. In the following studies, we will further analyze both the role of critical hyperparameter and the superiority of the SCTFA-SNN model under different conditions.

C. Impacts of Hyperparameter κ_τ

In the SCTFA-SNN model, the decay factor κ_τ is a critical hyperparameter that impacts the historically accumulated spatial-channel information. A natural question that arises is how the hyperparameter κ_τ influences the performance of the SCTFA-SNN model. To address this issue, we carry out comprehensive experiments for the SCTFA-SNN model on three datasets, and the results are presented in Figs. 6(a)-6(c), respectively. From the theoretical viewpoint, a very small κ_τ means that the historical information cannot be effectively accumulated due to a rapid decay. On the contrary, an extremely large κ_τ may introduce a certain amount of early irrelevant or redundant spatial-channel information for locating regions of interest. It is obvious that both of these two cases tend to deteriorate the performance of the SCTFA-SNN model. Consistent with this analysis, our results demonstrate that the SCTFA-SNN model can achieve the best accuracy at an intermediate value of κ_τ on all datasets. However, we notice that the optimal hyperparameter κ_τ may change across datasets. As shown in Figs. 6(a)-6(c), the SCTFA-SNN model can achieve the best performance at $\kappa_\tau = 0.4$ and 0.5 on the SL-Animals-DVS and MNIST-DVS, whereas a slightly larger $\kappa_\tau = 0.7$ is required to obtain the highest accuracy on the DVS Gesture. We speculate that the change of optimal κ_τ may be caused by multiple factors, such as different target movement speeds and different settings of other hyperparameters in these datasets.

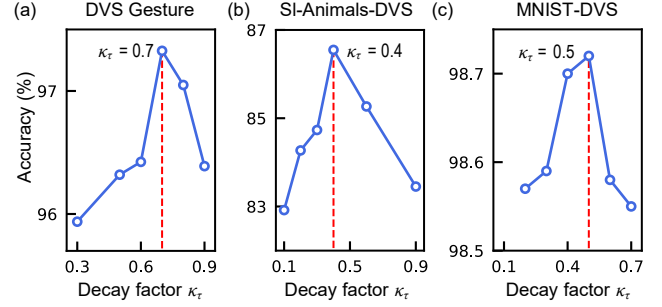


Fig. 6. Average top-1 accuracy of the SCTFA-SNN model at different values of hyperparameter κ_τ on three datasets. (a) DVS Gesture, (b) SL-Animals-DVS and (c) MNIST-DVS.

D. Robustness to Noisy Data

For SNN models, a high robustness to noisy data is essential for ensuring efficient information processing [47]. To evaluate the model robustness to unavoidable noise, we examine the performance of the best pre-trained groups of SNN models (10 independent models) by using noisy data. We assume that the noise satisfies Poisson distribution, which is believed to be a typical form of noise for event streams [58]. Specifically, we add noisy spiking events governed by a Poisson rate λ to event streams in the test set. A larger λ represents a stronger level of noise. In Fig. 7(a), we schematically shows an example of a frame-based data in the DVS Gesture mixed with the Poisson noise under different levels.

Our results depicted in Figs. 7(b)-(d) demonstrate that the SCTFA-SNN shows outstanding robustness to noise in comparison with different SNN models on all three datasets. As parameter λ is increased, we find that the average accuracy of different SNN models basically decreases, and the SCTFA-SNN displays substantial superiority for most cases, especially at intermediate noise levels. However, for extremely strong noise, the advantage of the SCTFA-SNN model is largely weakened. In reality, this is not so surprising because useful information represented as sparsely asynchronous events is drowned under strong noise conditions. For a more insightful analysis, we compute the Euclidean distance between the activation of the last convolutional layer of the original data and those of the noisy data using the same models, and the results are also presented in Figs. 7(b)-(d). Compared with other SNN models, the SCTFA-SNN tends to reduce more significant Euclidean distance between the noisy patterns and original patterns on different datasets. These observations suggest that the SCTFA module can help the SNNs fight against stochastic perturbations, thus endowing them with high robustness to noisy data.

E. Stability to Incomplete Data

Missing data are a vital factor that impacts the stability of SNN models and can be caused by different reasons. To examine our model performance on incomplete data, we consider two typical data loss scenarios: event loss and frame loss. For the case of event loss, we randomly remove sparse events from the original data with an event loss rate, whereas for the

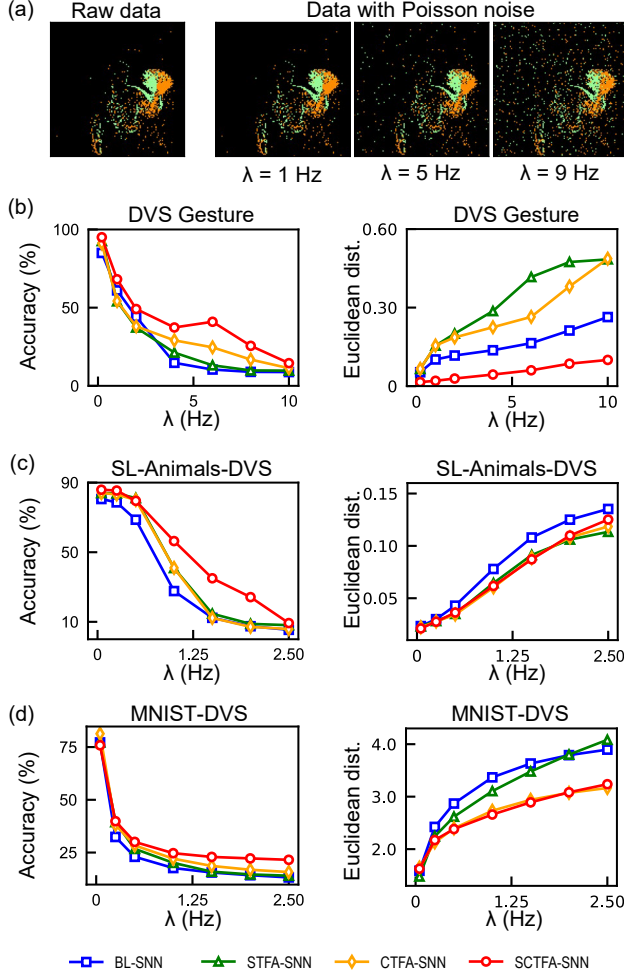


Fig. 7. Robustness of different SNN models to Poisson noise on three datasets. (a) An example of frame-based data in the DVS Gesture mixed with different noise levels (λ). The average accuracy of BL-SNN (blue), STFA-SNN (green), CTFA-SNN (orange) and SCTFA-SNN (red) models at different noise strengths is shown for the DVS Gesture (b), SL-Animals-DVS (c) and MNIST-DVS (d). In addition, the average Euclidean distances between the hidden activation (neuronal membrane potentials in the last convolutional layer) of original data and those of the noisy data over the time step is also plotted for different datasets.

frame loss, event-based frames are randomly dropped with a frame loss rate. Similarly, the best pre-trained group of SNN models is employed to assess their performance on incomplete data. In Figs. 8(a)-8(c), we present the average accuracy of different SNN models for both event loss (left) and frame loss (right) on three datasets. As expected, the performance of different SNN models decreases with increasing event and frame loss rates. On all datasets, the SCTFA-SNN model can stably maintain higher accuracy than that of the BL-SNN, STFA-SNN, and CTFA-SNN models for all event and frame loss rates. Compared with the event loss, we identify that the superiority of the SCTFA-SNN model is much more noticeable than the case of frame loss. This might be because event loss deteriorates the information representation for all input frames, whereas frame loss does not impact the information representation of the data used. Overall, our findings indicate an excellent stability of the SCTFA-SNN model to incomplete

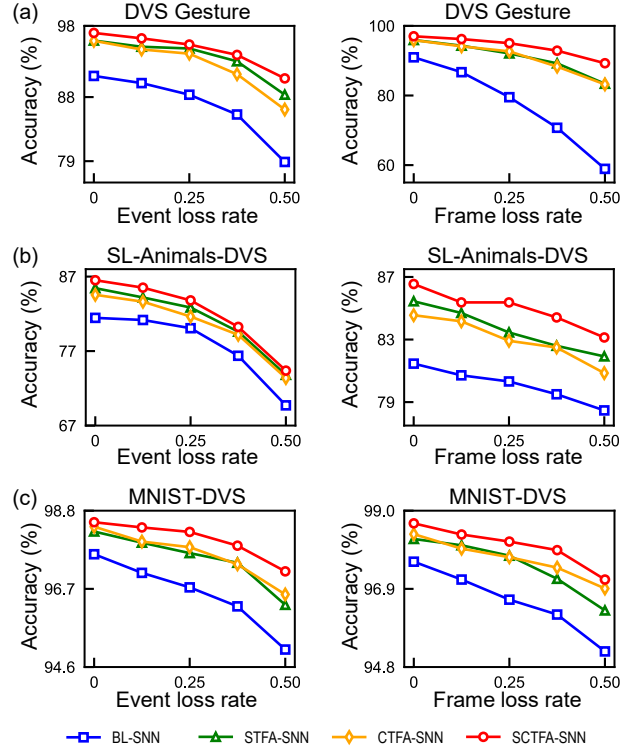


Fig. 8. Performance of the BL-SNN (blue), STFA-SNN (green), CTFA-SNN (orange) and SCTFA-SNN (red) models at different event (left) and frame (right) loss rates on three datasets. For both data loss scenarios, we consider that the loss rate is within the range of 0 and 0.50. (a) DVS Gesture, (b) SL-Animals-DVS and (c) MNIST-DVS.

TABLE IV
COMPLEXITY AND EFFICIENCY OF BL-SNN, STFA-SNN, CTFA-SNN AND SCTFA-SNN MODELS ON DIFFERENT DATASETS. HERE WE LIST THE NUMBER OF PARAMETERS, MULT-ADDS AND ACTUAL INFERENCE TIME PER BATCH.

Dataset	Model	Params ($\times 10^6$)	Mult-Adds ($\times 10^9$)	Inference time (ms)
DVS Gesture	BL-SNN	0.895	2.522	20.100
	STFA-SNN	0.896	2.529	24.153
	CTFA-SNN	0.936	2.523	26.422
	SCTFA-SNN	0.937	2.530	31.778
SL-Animals-DVS	BL-SNN	2.962	27.165	171.262
	STFA-SNN	2.963	27.207	193.425
	CTFA-SNN	3.126	27.170	192.663
	SCTFA-SNN	3.127	27.212	214.424
MNIST-DVS	BL-SNN	4.316	1.096	71.473
	STFA-SNN	4.317	1.101	81.642
	CTFA-SNN	4.327	1.096	80.142
	SCTFA-SNN	4.327	1.101	90.481

data.

F. Analysis of Complexity and Efficiency

It is obvious that introducing the SCTFA module into SNNs will cause a trade-off between the cost and performance. To further analyze the model complexity and efficiency, we calculate the numbers of parameters, multiply-add operations (Mult-Adds) and actual inference time per batch for the BL-SNN

TABLE V
A DETAILED COMPARISON BETWEEN THE SCTFA-SNN MODEL WITH OTHER EXISTING SNN WORKS ON DIFFERENT DATASETS.

Dataset	Model	Neuron type	Network architecture	Method	Accuracy
DVS Gesture	Zheng et al. (2021) [50]	LIF	ResNet17	STBP	96.87%
	Fang, et al. (2021) [48]	LIF	8-layer Spiking CNN	STBP	97.57%
	Wu et al. (2021) [49]	LIAF	5-layer Spiking CNN	BPTT	97.56%
	Yao et al. (2021) [29]	LIF	5-layer Spiking CNN	STBP + TA	95.49%
	Yao et al. (2021) [29]	LIAF	5-layer Spiking CNN	BPTT + TA	98.61%
	Sun et al. (2022) [59]	LIF	7-layer Spiking CNN	STL-STBP	97.22%
	Baldwin et al. (2021) [60]	GELU	GoogLeNet	BP	96.20%
	Sabater et al. (2022) [61]	ReLU	EvT	BP	96.20%
	Shrestha et al. (2018) [39]	SRM	8-layer Spiking CNN	SLAYER	93.64 \pm 0.49%
	Kugele et al. (2020) [52]	IF	DenseNet	ANN-SNN	95.56 \pm 0.14%
	Zhu et al. (2021) [62]	C-LIF	LeNet	STBP	95.83 \pm 0.28%
	Sun et al. (2022) [59]	LIF	7-layer Spiking CNN	STL-STBP	96.84 \pm 0.24%
	Wu et al. (2022) [47]	LIF	9-layer Spiking CNN	HP	97.01 \pm 0.21%
	Our work (Best top-1)	LIF	7-layer Spiking CNN	STBP + SCTFA	97.92%
	Our work (Average top-1)	LIF	7-layer Spiking CNN	STBP + SCTFA	97.33 \pm 0.58%
SL-Animals-DVS	Baldwin et al. (2021) [60]	GELU	GoogLeNet	BP	85.10%
	Sabater et al. (2022) [61]	ReLU	EvT	BP	88.12%
	Vasudevan et al. (2020) [45]	SRM	4-layer Spiking CNN	STBP	56.20 \pm 1.52%
	Vasudevan et al. (2020) [45]	SRM	4-layer Spiking CNN	SLAYER	60.09 \pm 4.58%
	Vasudevan et al. (2022) [42]	SRM	5-layer Spiking CNN	DECOLLE	70.60 \pm 7.80%
	Our work (Best top-1)	LIF	7-layer Spiking CNN	STBP + SCTFA	90.04%
	Our work (Average top-1)	LIF	7-layer Spiking CNN	STBP + SCTFA	86.55 \pm 1.66%
MNIST-DVS	Paulun et al. (2018) [63]	LIF	Retinotopic mapping	STDP + BP	90.56% (scale-4)
	Cannici et al. (2019) [64]	LSTM	4-layer ConvLSTM	BPTT	98.30% (scale-4)
	Sun et al. (2022) [59]	LIF	7-layer Spiking CNN	STL-STBP	98.70% (scale-4)
	Wang et al. (2021) [65]	IF	4-layer Spiking CNN	Tempotron	82.65% (scale-16)
	Liu et al. (2022) [31]	LIF	4-layer Spiking CNN	STBP	96.64%
	Zhu et al. (2021) [62]	C-LIF	LeNet	STBP	98.40 \pm 0.27% (scale-4)
	Sun et al. (2022) [59]	LIF	7-layer Spiking CNN	STL-STBP	98.37 \pm 0.17% (scale-4)
	Our work (Best top-1)	LIF	5-layer Spiking CNN	STBP + SCTFA	98.90% (scale-4)
	Our work (Average top-1)	LIF	5-layer Spiking CNN	STBP + SCTFA	98.72 \pm 0.14% (scale-4)

and SNNs with different attention modules. As comparisons shown in Tab. IV, the SCTFA module will introduce slightly more parameters and computational complexity into SNNs than the CTFA and STFA modules. For SNNs with different attention modules, such enhancement of computational complexity leads to a relatively long, but reasonable, increase in actual inference time. This non-negligible efficiency loss may be attributed to the increased element-wise operations and reduced parallelism degree due to the insert of attention modules. During the inference process, we find that the STFA-SNN and CTFA-SNN models exhibit the similar level of inference time on all datasets. In comparison with the BL-SNN model, the most complicated SCTFA-SNN model spends an extra inference time of 11.678 ms, 43.162 ms and 19.008 ms per batch on the DVS Gesture, SL-Animals-DVS and MNIST-DVS, respectively [Tab. IV]. Considering the length of event stream data used in this study, we believe that the realistic runtime of the SCTFA-SNN model is still acceptable for real applications. Altogether, our above analysis suggests that the proposed SCTFA-SNN can achieve superior performance, while maintaining a certain degree of competitive on complexity and efficiency.

G. Comparison with Prior SOTA Methods

Finally, we compare the proposed SCTFA-SNN model against other existing SOTA works. For a fair comparison, we mainly include results of SNNs with signal transmission via binary spikes, but exclude those with data augmentation. The comparison of accuracy among various works is summarized in Tab. V. Obviously, the SCTFA-SNN model can achieve the SOTA results on both the SL-Animals-DVS (average: 86.55 \pm 1.66%; best: 90.04%) and MNIST-DVS (average: 98.72 \pm 0.14%; best: 98.90%). In particular, we get a considerable increase of 15.95% on average over the prior best SNN model on the SL-Animals-DVS [42], and our SCTFA-SNN model even surpasses the current best non-SNN method referred to event transformer (EvT) by 1.92% accuracy [61]. On the DVS Gesture, our best result (97.92%) obtained at $T = 10$ is slightly lower than a recent reported SOTA accuracy (98.61%) with a larger timestep of $T = 60$ [29]. However, the SOTA accuracy achieved in this study is achieved by using the leaky integrate and analog fire (LIAF) neurons [29], [49], with their signal transmission via analog values but not binary spikes. Indeed, the performance of our model is better than that of the corresponding SNN with spiking LIF neurons (95.49%), which is also reported in the same work [see Tab. V] [61]. These results imply that our SCTFA-SNN model

is competitive with other existing methods, and the proposed SCTFA module can remarkably improve the performance of SNNs by fusing the spatial, channel and temporal information altogether.

V. CONCLUSIONS

As an emerging field in artificial intelligence, SNNs have gained more and more attentions and is arousing the wave of neuromorphic computing [1]–[3], [6]–[10]. There is a broad consensus that the development of highly efficient SNN models should adequately learn from brain mechanisms [4], [5], [10], [66]. Visual attention is essential for human perception [16], [17]. Recently, a few studies devoted to introduce attention mechanisms into SNNs to extract important information in spatial, temporal and channel dimensions separately [29]–[32], but none of them considered to comprehensively use the information from all dimensions together. In this work, we designed a friendly plug-and-play SCTFA module for SNNs by borrowing the idea from the predictive remapping of attentions [33]–[38]. Unlike other attention mechanisms inserted in previous SNN models, the main novelty of our approach allows SNNs to make full use of historical spatial-channel information accumulated in the temporal domain to efficiently predict current attention regions. Through experiments, we identified that the SCTFA-SNN model not only achieves higher accuracy than other two SNN models with the degenerated spatial-temporal-fused or channel-temporal-fused attention modules, but also shows the competitive performance with existing SOTA results on various event stream datasets. In addition, our analysis also showed that our SCTFA-SNN model exhibits excellent robustness and stability under different conditions, despite increasing a certain degree of complexity and inference time.

Our findings presented in this study emphasize that appropriately incorporating brain-inspired computational principles can improve the information processing capability of SNNs. In future studies, we plan to train the SCTFA-SNN with more efficient hybrid or synergistic learning strategies [47], [59]. Moreover, we also hope to further generalize the SCTFA-SNN model to other challenging intelligent applications and realize this model on neuromorphic chip.

REFERENCES

- [1] W. Maass, “Networks of spiking neurons: the third generation of neural network models,” *Neural Netw.*, vol. 10, no. 9, pp. 1659–1671, 1997.
- [2] S. Ghosh-Dastidar and H. Adeli, “Spiking neural networks,” *Int. J. Neural Syst.*, vol. 19, no. 04, pp. 295–308, 2009.
- [3] A. Tavanaei, M. Ghodrati, S. R. Kheradpisheh, T. Masquelier, and A. Maida, “Deep learning in spiking neural networks,” *Neural Netw.*, vol. 111, pp. 47–63, 2019.
- [4] X. Cheng, Y. Hao, J. Xu, and B. Xu, “LISNN: Improving spiking neural networks with lateral interactions for robust object recognition,” in *Proc. Int. Joint Conf. Artif. Intell. (IJCAI)*, Jul. 2020, pp. 1519–1525.
- [5] J. Pei, L. Deng, S. Song, M. Zhao, Y. Zhang, S. Wu, G. Wang, Z. Zou, Z. Wu, W. He *et al.*, “Towards artificial general intelligence with hybrid Tianjic chip architecture,” *Nature*, vol. 572, no. 7767, pp. 106–111, 2019.
- [6] Z. Yang, Y. Wu, G. Wang, Y. Yang, G. Li, L. Deng, J. Zhu, and L. Shi, (2019) DashNet: a hybrid artificial and spiking neural network for high-speed object tracking. [Online]. Available: <https://doi.org/10.48550/arXiv.1909.12942>
- [7] S. Kim, S. Park, B. Na, and S. Yoon, “Spiking-YOLO: spiking neural network for energy-efficient object detection,” in *Proc. Conf. AAAI Artif. Intell. (AAAI)*, vol. 34, no. 07, Apr. 2020, pp. 11 270–11 277.
- [8] S. A. Lobov, A. N. Mikhaylov, M. Shamshin, V. A. Makarov, and V. B. Kazantsev, “Spatial properties of STDP in a self-learning spiking neural network enable controlling a mobile robot,” *Front. Neurosci.*, vol. 14, no. 88, pp. 1–10, Feb. 2020.
- [9] Z. Bing, C. Meschede, F. Röhrbein, K. Huang, and A. C. Knoll, “A survey of robotics control based on learning-inspired spiking neural networks,” *Front. Neurosci.*, vol. 12, no. 35, pp. 1–22, Jul. 2018.
- [10] E. Nichols, L. J. McDaid, and N. Siddique, “Biologically inspired SNN for robot control,” *IEEE Trans. Cybern.*, vol. 43, no. 1, pp. 115–128, 2012.
- [11] D. Xing, Y. Yang, T. Zhang, and B. Xu, “A Brain-Inspired Approach for Probabilistic Estimation and Efficient Planning in Precision Physical Interaction,” *IEEE Trans. Cybern.*, 2022.
- [12] Y. Wu, L. Deng, G. Li, J. Zhu, and L. Shi, “Spatio-temporal backpropagation for training high-performance spiking neural networks,” *Front. Neurosci.*, no. 331, pp. 1–12, May 2018.
- [13] Y. Wu, L. Deng, G. Li, J. Zhu, Y. Xie, and L. Shi, “Direct training for spiking neural networks: faster, larger, better,” in *Proc. Conf. AAAI Artif. Intell. (AAAI)*, vol. 33, no. 01, Jul. 2019, pp. 1311–1318.
- [14] B. Rueckauer, I.-A. Lungu, Y. Hu, M. Pfeiffer, and S.-C. Liu, “Conversion of continuous-valued deep networks to efficient event-driven networks for image classification,” *Front. Neurosci.*, vol. 11, no. 682, pp. 1–12, Dec. 2017.
- [15] P. U. Diehl, D. Neil, J. Binas, M. Cook, S.-C. Liu, and M. Pfeiffer, “Fast-classifying, high-accuracy spiking deep networks through weight and threshold balancing,” in *Proc. Int. Jt. Conf. Neural Netw. (IJCNN)*, IEEE, 2015, pp. 1–8.
- [16] M. Carrasco, “Visual attention: The past 25 years,” *Vision Res.*, vol. 51, no. 13, pp. 1484–1525, 2011.
- [17] V. A. Lamme, “Why visual attention and awareness are different,” *Trends Cogn. Sci.*, vol. 7, no. 1, pp. 12–18, 2003.
- [18] J. Hu, L. Shen, and G. Sun, “Squeeze-and-excitation networks,” in *Proc. IEEE Conf. Comput. Vis. Pattern Recognit. (CVPR)*, Jun. 2018.
- [19] Q. Wang, B. Wu, P. Zhu, P. Li, W. Zuo, and Q. Hu, “ECA-Net: Efficient channel attention for deep convolutional neural networks,” in *Proc. IEEE Conf. Comput. Vis. Pattern Recognit. (CVPR)*, Computer Vision Foundation / IEEE, 2020, pp. 11 531–11 539.
- [20] M. Jaderberg, K. Simonyan, A. Zisserman *et al.*, “Spatial transformer networks,” *Adv. Neural Inf. Proces. Syst.*, vol. 8, pp. 1–9, 2015.
- [21] X. Wang, R. Girshick, A. Gupta, and K. He, “Non-local neural networks,” in *Proc. IEEE Conf. Comput. Vis. Pattern Recognit. (CVPR)*, Jun. 2018, pp. 7794–7803.
- [22] J. Shen, X. Tang, X. Dong, and L. Shao, “Visual object tracking by hierarchical attention siamese network,” *IEEE Trans. Cybern.*, vol. 50, no. 7, pp. 3068–3080, 2019.
- [23] S. Xu, Y. Cheng, K. Gu, Y. Yang, S. Chang, and P. Zhou, “Jointly attentive spatial-temporal pooling networks for video-based person re-identification,” in *Proc. IEEE Int. Conf. Coput. Vis.*, Oct. 2017.
- [24] R. Zhang, J. Li, H. Sun, Y. Ge, P. Luo, X. Wang, and L. Lin, “SCAN: Self-and-cotive attention network for video person re-identification,” *IEEE T. Image Process.*, vol. 28, no. 10, pp. 4870–4882, 2019.
- [25] S. Woo, J. Park, J.-Y. Lee, and I. S. Kweon, “CBAM: Convolutional block attention module,” in *Proc. Eur. Conf. Comp. Vis. (ECCV)*, Sep. 2018, pp. 3–19.
- [26] L. Chen, H. Zhang, J. Xiao, L. Nie, J. Shao, W. Liu, and T.-S. Chua, “SCA-CNN: Spatial and channel-wise attention in convolutional networks for image captioning,” in *Proc. IEEE Conf. Comput. Vis. Pattern Recognit. (CVPR)*, Jul. 2017, pp. 5659–5667.
- [27] L. Gao, X. Li, J. Song, and H. T. Shen, “Hierarchical LSTMs with adaptive attention for visual captioning,” *IEEE Trans. Pattern Anal. Mach. Intell.*, vol. 42, no. 5, pp. 1112–1131, 2019.
- [28] S. Song, C. Lan, J. Xing, W. Zeng, and J. Liu, “An end-to-end spatio-temporal attention model for human action recognition from skeleton data,” in *Proc. Conf. AAAI Artif. Intell. (AAAI)*, vol. 31, no. 1, 2017, pp. 4263–4270.
- [29] M. Yao, H. Gao, G. Zhao, D. Wang, Y. Lin, Z. Yang, and G. Li, “Temporal-wise attention spiking neural networks for event streams classification,” in *Proc. IEEE/CVF Int. Conf. Comp. Vis. (ICCV)*, Oct. 2021, pp. 10 221–10 230.
- [30] S. Kundu, G. Datta, M. Pedram, and P. A. Beerel, “Spike-thrift: Towards energy-efficient deep spiking neural networks by limiting spiking activity via attention-guided compression,” in *IEEE Winter Conf. Appl. Comput. Vis. (WACV)*, 2021, pp. 3953–3962.

- [31] Q. Liu, D. Xing, L. Feng, H. Tang, and G. Pan, "Event-based multimodal spiking neural network with attention mechanism," in *IEEE Intl. Conf. on Acoustics, Speech and Signal Processing (ICASSP)*. IEEE, 2022, pp. 8922–8926.
- [32] X. Liu, M. Yan, L. Deng, Y. Wu, D. Han, G. Li, X. Ye, and D. Fan, "General spiking neural network framework for learning trajectory from noisy mmwave radar," *Neuromorph. Comput. Eng.*, 2022.
- [33] D. Melcher, "Predictive remapping of visual features precedes saccadic eye movements," *Nat. Neurosci.*, vol. 10, no. 7, pp. 903–907, 2007.
- [34] S. Mathôt and J. Theeuwes, "Evidence for the predictive remapping of visual attention," *Exp. Brain. Res.*, vol. 200, no. 1, pp. 117–122, 2010.
- [35] M. Rolfs, D. Jonikaitis, H. Deubel, and P. Cavanagh, "Predictive remapping of attention across eye movements," *Nat. Neurosci.*, vol. 14, no. 2, pp. 252–256, Dec. 2011.
- [36] M. Szinte, D. Jonikaitis, D. Rangelov, and H. Deubel, "Pre-saccadic remapping relies on dynamics of spatial attention," *Elife*, vol. 7, no. e37598, pp. 1–16, 2018.
- [37] J. P. Wilmott and M. M. Michel, "Transsaccadic integration of visual information is predictive, attention-based, and spatially precise," *J. Vis.*, vol. 21, no. 8, pp. 1–26, Jul. 2021.
- [38] J. D. Golomb and J. A. Mazer, "Visual remapping," *Annu. Rev. Vis. Sci.*, vol. 7, pp. 257–277, 2021.
- [39] S. B. Shrestha and G. Orchard, "SLAYER: Spike layer error reassignment in time," *Adv. Neural Inf. Process. Syst.*, vol. 31, 2018.
- [40] P. J. Werbos, "Backpropagation through time: what it does and how to do it," *P. IEEE*, vol. 78, no. 10, pp. 1550–1560, 1990.
- [41] A. Amir, B. Taba, D. Berg, T. Melano, J. McKinstry, C. Di Nolfo, T. Nayak, A. Andreopoulos, G. Garreau, M. Mendoza *et al.*, "A low power, fully event-based gesture recognition system," in *Proc. IEEE Conf. Comput. Vis. Pattern Recognit. (CVPR)*, 2017, pp. 7243–7252.
- [42] A. Vasudevan, P. Negri, C. Di Ielsi, B. Linares-Barranco, and T. Serrano-Gotarredona, "SL-Animals-DVS: event-driven sign language animals dataset," *Pattern Anal. Appl.*, vol. 25, no. 3, pp. 505–520, 2022.
- [43] T. Serrano-Gotarredona and B. Linares-Barranco, "Poker-DVS and MNIST-DVS. their history, how they were made, and other details," *Front. Neurosci.*, vol. 9, no. 481, 2015.
- [44] T. Serrano-Gotarredona and B. Linares-Barranco, "A 128×128 1.5% contrast sensitivity 0.9% FPN 3 μ s latency 4 mW asynchronous frame-free dynamic vision sensor using transimpedance preamplifiers," *IEEE J. Solid-State Circuits*, vol. 48, no. 3, pp. 827–838, 2013.
- [45] A. Vasudevan, P. Negri, B. Linares-Barranco, and T. Serrano-Gotarredona, "Introduction and analysis of an event-based sign language dataset," in *Proc. Int. Conf. Autom. Face Gesture. Recognit.* IEEE, 2020, pp. 675–682.
- [46] J. H. Lee, T. Delbruck, and M. Pfeiffer, "Training deep spiking neural networks using backpropagation," *Front. Neurosci.*, vol. 10, no. 508, pp. 1–13, Nov. 2016.
- [47] Y. Wu, R. Zhao, J. Zhu, F. Chen, M. Xu, G. Li, S. Song, L. Deng, G. Wang, H. Zheng *et al.*, "Brain-inspired global-local learning incorporated with neuromorphic computing," *Nat. Commun.*, vol. 13, no. 1, pp. 1–14, 2022.
- [48] W. Fang, Z. Yu, Y. Chen, T. e. Masquelier, T. Huang, and Y. Tian, "Incorporating learnable membrane time constant to enhance learning of spiking neural networks," in *Proc. IEEE/CVF Int. Conf. Comp. Vis. (ICCV)*, Oct. 2021, pp. 2661–2671.
- [49] Z. Wu, H. Zhang, Y. Lin, G. Li, M. Wang, and Y. Tang, "LIAF-Net: Leaky integrate and analog fire network for lightweight and efficient spatiotemporal information processing," *IEEE Trans. Neural Netw. Learn. Syst.*, pp. 1–14, 2021.
- [50] H. Zheng, Y. Wu, L. Deng, Y. Hu, and G. Li, "Going deeper with directly-trained larger spiking neural networks," in *Proc. Conf. AAAI Artif. Intell. (AAAI)*, vol. 35, no. 12, May 2021, pp. 11 062–11 070.
- [51] W. He, Y. Wu, L. Deng, G. Li, H. Wang, Y. Tian, W. Ding, W. Wang, and Y. Xie, "Comparing SNNs and RNNs on neuromorphic vision datasets: Similarities and differences," *Neural Netw.*, vol. 132, pp. 108–120, Dec. 2020.
- [52] A. Kugele, T. Pfeil, M. Pfeiffer, and E. Chicca, "Efficient processing of spatio-temporal data streams with spiking neural networks," *Front. Neurosci.*, vol. 14, no. 439, pp. 1–13, May 2020.
- [53] G. Shen, D. Zhao, and Y. Zeng. (2022) EventMix: An efficient augmentation strategy for event-based data. [Online]. Available: <https://doi.org/10.48550/arXiv.2205.12054>
- [54] F. Gu, W. Sng, X. Hu, and F. Yu, "EventDrop: Data augmentation for event-based learning," in *Proc. Int. Joint Conf. Artif. Intell. (IJCAI)*, Aug. 2021, pp. 700–707.
- [55] W. Gerstner, W. M. Kistler, R. Naud, and L. Paninski, *Neuronal dynamics: From single neurons to networks and models of cognition*. Cambridge University Press, 2014.
- [56] A. G. Roy, N. Navab, and C. Wachinger, "Concurrent spatial and channel'squeeze & excitation'in fully convolutional networks," in *Med. Image Comput. Comput. Assist. Interv.* Springer, 2018, pp. 421–429.
- [57] A. Chattopadhyay, A. Sarkar, P. Howlader, and V. N. Balasubramanian, "Grad-CAM++: Generalized gradient-based visual explanations for deep convolutional networks," in *IEEE Winter Conf. Appl. Comput. Vis. (WACV)*. IEEE, 2018, pp. 839–847.
- [58] A. Khodamoradi and R. Kastner, "O(N)-space spatiotemporal filter for reducing noise in neuromorphic vision sensors," *IEEE Trans. Emerg. Top. Comput.*, vol. 9, no. 1, pp. 15–23, 2018.
- [59] H. Sun, W. Cai, B. Yang, Y. Cui, Y. Xia, D. Yao, and D. Guo. (2022) A synapse-threshold synergistic learning approach for spiking neural networks. [Online]. Available: <https://doi.org/10.48550/arXiv.2206.06129>
- [60] R. Baldwin, R. Liu, M. M. Almatrafi, V. K. Asari, and K. Hirakawa, "Time-ordered recent event (TORE) volumes for event cameras," *IEEE Trans. Pattern Anal. Mach. Intell.*, vol. 14, no. 8, pp. 1–14, Aug. 2022.
- [61] A. Sabater, L. Montesano, and A. C. Murillo, "Event Transformer: A sparse-aware solution for efficient event data processing," in *Proc. IEEE Conf. Comput. Vis. Pattern Recognit. (CVPR)*, Jun. 2022, pp. 2677–2686.
- [62] X. Zhu, B. Zhao, D. Ma, and H. Tang, "An efficient learning algorithm for direct training deep spiking neural networks," *IEEE Trans. Cogn. Dev. Syst.*, pp. 1–10, 2021.
- [63] L. Paulun, A. Wendt, and N. Kasabov, "A retinotopic spiking neural network system for accurate recognition of moving objects using NeuCube and dynamic vision sensors," *Front. Comput. Neurosci.*, vol. 12, no. 42, pp. 1–13, June 2018.
- [64] M. Cannici, M. Ciccone, A. Romanoni, and M. Matteucci, "Attention mechanisms for object recognition with event-based cameras," in *IEEE Winter Conf. Appl. Comput. Vis. (WACV)*. IEEE, 2019, pp. 1127–1136.
- [65] T. Wang, C. Shi, X. Zhou, Y. Lin, J. He, P. Gan, P. Li, Y. Wang, L. Liu, N. Wu *et al.*, "CompSNN: A lightweight spiking neural network based on spatiotemporally compressive spike features," *Neurocomputing*, vol. 425, pp. 96–106, 2021.
- [66] D. Liu and S. Yue, "Event-driven continuous STDP learning with deep structure for visual pattern recognition," *IEEE Trans. Cybern.*, vol. 49, no. 4, pp. 1377–1390, 2018.